^{1}H, ^{13}C, and ^{15}N Resonance Assignments and Secondary Structure Analysis of the HU Protein from *Bacillus stearothermophilus* Using Two- and Three-Dimensional Double- and Triple-Resonance Heteronuclear Magnetic Resonance Spectroscopy†

Hans Vis,‡ Rolf Boelens,*,‡ Matteo Mariani,§ Ralf Stroop,‡ Constantin E. Vorgias,|| Keith S. Wilson,|| and Robert Kaptein‡

Bijvoet Center for Biomolecular Research, Utrecht University, Padualaan 8, 3584 CH Utrecht, The Netherlands, and European Molecular Biology Laboratory (EMBL), c/o DESY, Notkestrasse 85, D-22603 Hamburg, Germany

Received July 21, 1994; Revised Manuscript Received September 19, 1994⊗

ABSTRACT: Nearly complete ^{1}H, ^{13}C, and ^{15}N resonance assignments have been obtained for the protein HU from *Bacillus stearothermophilus* (dimer, 19.5 kDa) using double- and triple-resonance 2D and 3D NMR experiments. This has resulted in assignments of 91% of the observable protons, 98% of all ^{13}C, and 92% of all ^{15}N nuclei. NOEs obtained from a 3D time-shared NOESY-(^{13}C,^{15}N)-HSQC spectrum, exchange data of amide protons, and chemical shifts of the $^{1}H^{\alpha}$, $^{1}H^{N}$, $^{13}C^{\beta}$, $^{13}C^{\alpha}$, ^{13}CO, and ^{15}N nuclei have been used to identify the secondary structure elements. Three α-helices (residues 3−13, 18−37, and 83−90) and three extended strands (residues 40−45, 48−62, and 67−82) have been found in HU. The arrangement of these elements of secondary structure is very similar to the X-ray structure [Tanaka et al. (1984) *Nature 310*, 376−381; White et al. (1989) *Proteins 5*, 281−288]. The conformation of the proposed DNA-binding region of HU, i.e., an antiparallel β-hairpin, was not observed previously in the X-ray structure. In the NMR structure long range NOEs in the β-arm region (residues 53−76) suggest a distortion between residue Pro-72 and Ala-73 and between Pro-63 and Gln-64 with concomitant distortions in the opposite strand. The NOE data indicate further that the loop region in the DNA-binding arms of HU is arranged as a type I β-turn from Pro-63 to Gly-66.

Prokaryotes contain small DNA-binding proteins, that are capable of bending DNA. Some of their biochemical properties resemble those of the eukaryotic histones, which play a major role in the compacting of the DNA into nucleosomes and eventually condensation into chromosomes. These bacterial proteins have the ability of compacting the DNA into nucleosome-like particles in which the DNA is negatively supercoiled (McGhee et al., 1980). However, the association of these proteins with the bulk DNA to form bacterial chromosomes is not fully understood, and more likely these proteins are localized in the border region with ribosomes where transcription and translation occur (Drlica et al., 1987; Kellenberger, 1988).

The protein HU binds nonspecifically to both single-stranded and double-stranded DNA as well as to RNA. Besides its feature of bending the DNA, it has been demonstrated biochemically that HU is involved in transcription activation, in site-specific recombination, and in initiation of DNA replication (Drlica et al., 1987). The fundamental unit of the HU protein in solution is a homotypic dimer. In some cases, for instance, in *Escherichia coli*, HU consists of two different monomers. The significant homology of the amino acid sequence of the HU subunits among different bacterial species is a strong indication of the similarity between their chemical structures.

HU of *Bacillus stearothermophilus* (HUBst) consists of two identical monomers of 90 residues and has a total molecular mass of 19.5 kDa. The primary structure of HUBst has been determined by Kimura and Wilson (1983). HUBst has been crystallized (Dijk et al., 1983), and a three-dimensional structure has been determined by X-ray crystallography (Tanaka et al., 1984), which has been refined to a resolution of 2.1 Å (White et al., 1989). The prominent structural characteristics of the HUBst dimer are a globular, mainly α-helical core, stabilized by hydrophobic contacts among hydrophobic amino acids. In addition, the dimer contains two antiparallel β-sheets from which a pair of extended β-ribbon arms protrude into the solvent, an appearance which is reminiscent of the arms of a lobster.

The most likely DNA-binding region of HU, as suggested by Tanaka (1984), incorporates the adjacent β-strands of both monomers and the flexible β-ribbon arms. These are complementary to either the major or the minor groove of double-stranded DNA. The arm regions, which are probably highly flexible and not visible in the original X-ray structure, are postulated to lie in the extended part of one of the grooves of the DNA. This general DNA-binding model is supported by a broad range of biochemical data, such as the conservation of lysine and arginine residues in the proposed DNA-binding region among different related proteins (Drlica et al., 1987), chemical modification studies with HUBst, involving the arginine residues in the β-arms (Lammi et al., 1984), and fluorescence studies on DNA−protein interactions with the homologous protein TF1 (Härd et al., 1989). Additionally, studies on DNA protection by the homologous

† This work was supported in part by the Netherlands Foundation for Chemical Research (SON) with financial support from the Netherlands Organization for Scientific Research (NWO).

* To whom correspondence should be addressed.

‡ Utrecht University.

§ On leave from Istituto di Biofisica, Facoltà di Medicina, Università di Genova, Via Giotto 2, Genova Sestri, Ponente, Italy.

|| EMBL.

⊗ Abstract published in *Advance ACS Abstracts,* November 1, 1994.

0006-2960/94/0433-14858$04.50/0 © 1994 American Chemical Society

integration host factor (IHF) provide indications for the minor groove as the preferential binding groove at the DNA with the β-ribbon arms (Goodman et al., 1990; Craig et al., 1984).

An NMR study of the HUBst dimer has been initiated with the aim of resolving the structure and dynamics of the DNA-binding region both free in solution and bound to DNA. With its 19.5 kDa HUBst cannot be considered a small protein for NMR and therefore a (^{13}C,^{15}N)-double-labeled protein was used. This facilitates analyses for both the assignment (Ikura et al., 1990) and the structure determination (Zuiderweg & Fesik, 1989; Marion et al., 1989a).

Here the complete ^{1}H, ^{13}C, and ^{15}N resonance assignments of HUBst are presented. The backbone assignment was accomplished using six 3D triple-resonance experiments correlating intraresidue and interresidue backbone nuclei, thus providing three independent methods for connecting adjacent nuclei. The identification of the aliphatic spin systems was accomplished using gradient-enhanced 3D HCCH-COSY and 3D HCCH-TOCSY experiments, yielding the ^{13}C and ^{1}H side chain resonances. Finally, most of the side chain NH_2 and C=O resonances were assigned.

The secondary structure elements of HUBst in solution were established using a 3D time-shared NOESY-(^{13}C,^{15}N)-HSQC spectrum and from an analysis of chemical shifts relative to the random coil value (Wishart et al., 1991). The secondary structure of the suggested DNA-binding arm, which was not observed in the X-ray structure, could be established. The arm contains irregularities at the well-conserved prolines, while the loop has been identified as a type I β-turn.

EXPERIMENTAL PROCEDURES

Sample Preparation. Cloning of the HUBst gene and overproduction of the protein were described by Padas et al. (1992). ^{13}C/^{15}N-labelled protein was prepared using ^{15}-NH_4Cl and [^{13}C]glucose in a minimal medium. The protein was purified employing affinity chromatography on heparin–Sepharose and Mono-S FPLC. The purity was over 95% as judged by SDS–PAGE and silver staining. The recombinant HU was as active as the protein purified from *B. stearothermophilus* with respect to its DNA-binding properties (Padas et al., 1992).

The protein was dissolved in a 50 mM phosphate buffer at pH 4.6 and 200 mM potassium chloride. NMR experiments were performed with one 2.2 mM protein sample in 95% $^{1}H_2O$/5% $^{2}H_2O$ at 311 K.

NMR Spectroscopy. NMR spectra were recorded on a Bruker AMX600 which was equipped with a triple-resonance probe with a shielded gradient coil. The 2D (^{15}N and ^{13}C) HSQC experiments were recorded as described by Norwood et al. (1990) and Bax et al. (1990a).

The constant-time versions of the HNCO, HNCA, and HN(CO)CA experiments were recorded essentially as described by Grzesiek et al. (1992), and the HN(CA)CO experiment was recorded as described by Clubb et al. (1992); a refocused INEPT was used for the magnetization transfer from ^{1}H to ^{15}N for the HNCA and the H(N)CACO experiments. A second 3D HNCO experiment was recorded with the adjustment of the (N,C′)-INEPT delay to select for NH_2 groups that are attached to carbonyl carbons and is referred to accordingly as the 3D H_2NCO experiment. Furthermore, 2D ^{15}N-filtered and 2D ^{13}CO-filtered versions of the HNCO experiment were recorded with the ^{13}CO and ^{15}N carrier positions at 167.65 and 98.59 ppm, respectively, allowing for the excitation of the side chain $^{13}C^{\zeta}$ and $^{15}N^{\epsilon}$ resonance frequencies of arginine residues (Yamazaki et al., 1993). In the following these experiments will be referred to as the 2D HN(CZ) and the 2D H(N)CZ experiments. On the basis of the H(N)CZ experiment a 2D H(NCZ)N was recorded in which the relayed transfer from Arg-$^{13}C^{\zeta}$ to Arg-$^{15}N^{\eta}$ was established via multiple quantum coherence. A 2D H(C)N was recorded essentially as described by Yamazaki et al. (1993) using composite pulse ^{1}H decoupling during the evolution of magnetization on ^{13}C and ^{15}N and using gradient coherence selection for aliphatic protons.

The 3D HCCH-COSY experiment was recorded as described by Bax et al. (1990b) using a constant-time method in t_2 for a better resolution and composite pulse ^{1}H decoupling instead of 180° pulses after transfer of magnetization to ^{13}C nuclei. The 3D HCCH-TOCSY experiments were recorded essentially as described by Bax et al. (1990c).

The HA(CACO)NH experiment was derived from the HBHA(CBCACO)NH experiment as described by Grzesiek & Bax (1993a), which was modified by removing the magnetization transfer between $^{13}C^{\alpha}$ and $^{13}C^{\beta}$ spins. Constant-time versions of the HCACO and the HCA(CO)N experiments were recorded essentially as described by Grzesiek & Bax (1993b). However, for the HCA(CO)N experiment the transfer from ^{13}CO to ^{15}N was established via multiple quantum coherence. In one 3D HCACO experiment, the delay during which anti-phase carbon magnetization with respect to protons was transferred to in-phase carbon magnetization, and vice versa, was adjusted to select for CH_2 groups attached to carbonyl carbons. To avoid confusion with the HCACO experiment, this experiment will hereafter be referred to as the 3D H_2CCO experiment.

The pulse sequences of the 3D time-shared TOCSY-(^{13}C,^{15}N)-HSQC, the 3D time-shared NOESY-(^{13}C,^{15}N)-HSQC, and the 3D time-shared (^{15}N)-HMQC-NOESY-(^{13}C,^{15}N)-HSQC experiments are shown in Figure 1, parts A, B, and C, respectively. Pulsed field gradients were used for the suppression of undesired signals (Hurd, 1990; Vuister et al., 1991; Bax & Pochapsky, 1992). The time-shared (^{13}C,^{15}N) chemical shift evolution, as originally suggested by Sørensen (1990) and Farmer (1991), allows the simultaneous recording of (^{13}C,^{1}H) and (^{15}N,^{1}H) correlations. Similar to the 2D time-shared (^{13}C,^{15}N)-HSQC (Boelens et al., 1994) these 3D time-shared (^{13}C,^{15}N) experiments result in a factor two faster recording of the 3D correlations, as compared to the separate 3D experiments. A related time-shared NOESY-(^{13}C,^{15}N)-HSQC experiment has recently been proposed by Pascal et al. (1994).

Fast exchange of amide protons with water is identified from the difference of a gradient enhanced (^{15}N)-HSQC experiment with and without presaturation.

Presaturation was used in all experiments to suppress the water signal, and additional spin-lock pulses in the HA(CACO)NH, HCCH-COSY, and HCCH-TOCSY experiments were applied to suppress magnetization of protons not attached to ^{13}C nuclei. Further improvement of water suppression in the HCCH-TOCSY experiments was attained by employing pulsed field gradients, as described by Kay at al. (1993). Resonances that are normally suppressed with the water signal were recovered in the HA(CACO)NH and

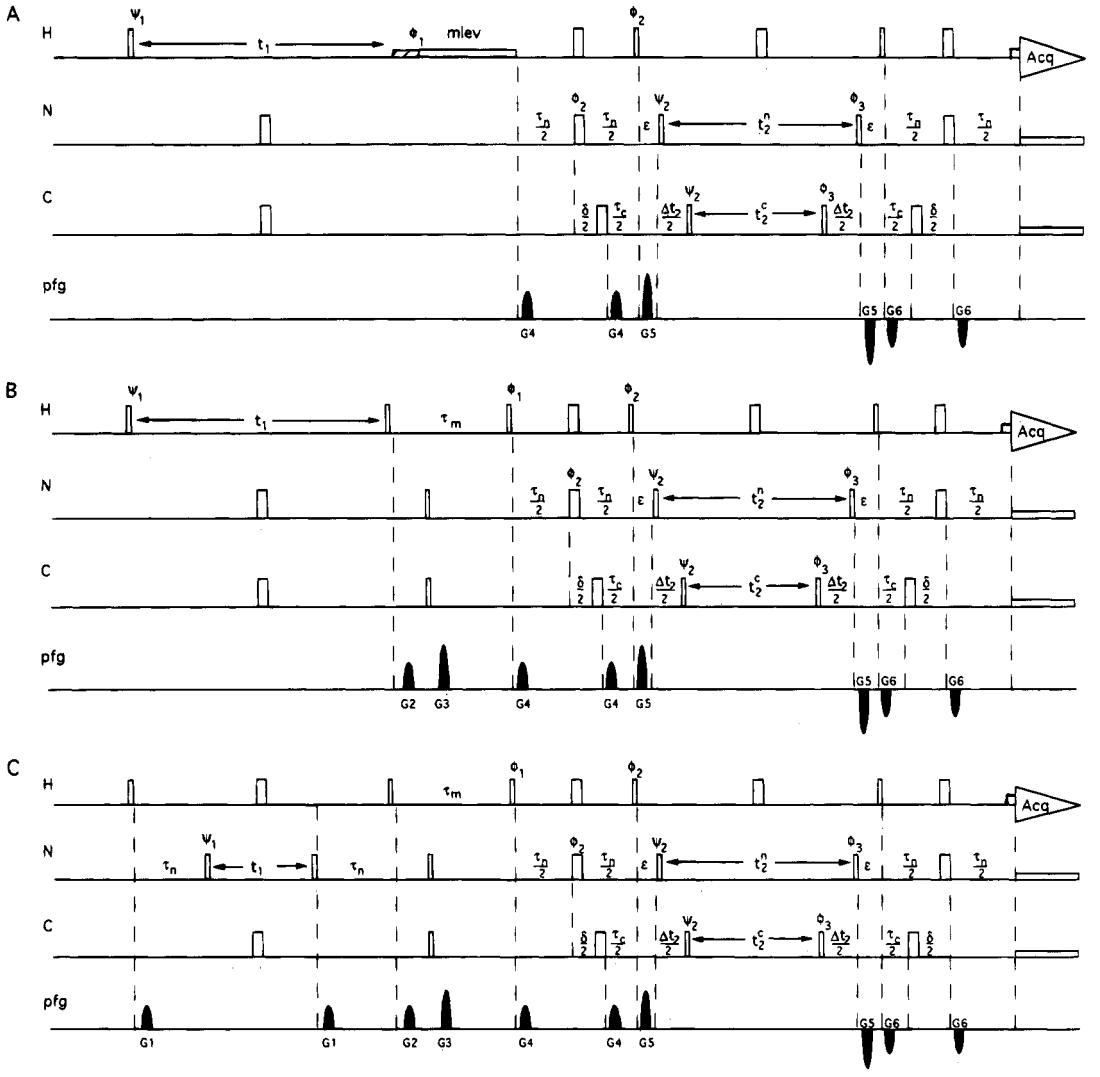

FIGURE 1: Pulse sequences of the 3D time-shared TOCSY-(^{13}C,^{15}N)-HSQC (A), the time-shared NOESY-(^{13}C,^{15}N)-HSQC (B), and the time-shared (^{15}N)-HMQC-NOESY-(^{13}C,^{15}N)-HSQC (C) experiments. For adequate suppression of artifacts, the sequences require a 8-step phase cycle: $\phi_1 = (4x, 4(-x))$, $\phi_2 = y$, $\phi_3 = (x, -x)$, $\psi_1 = (2x, 2(-x))$, $\psi_2 = x$, Acq $= x, 2(-x), x, -x, 2(-x), x$. The ^{13}C carrier is positioned in the middle of the aliphatic region. Quadrature in the F_1 and F_2 dimensions is obtained by applying the States-TPPI method to ψ_1 and ψ_2, respectively.

HCCH-COSY experiments using the SCUBA method (Brown et al., 1988). Phase sensitive detection in the indirectly detected dimensions was achieved according to the TPPI method (Marion et al., 1983) in the case of ^{1}H, ^{13}CO, or ^{15}N evolution and in the case of ^{13}C evolution according to the States-TPPI method (Marion et al., 1989). In most of the experiments the ^{1}H, ^{13}C, ^{13}CO, and ^{15}N carriers were positioned to obtain an unfolded spectrum with an optimal resolution for the desired signals. Folding was used to increase the resolution of the ^{13}C directions in the 3D HCCH, 3D TOCSY-HSQC, and 3D NOESY-HSQC experiments. Supplementary material is available that summarizes the NMR parameters used in the experiments as described above.

Forward linear prediction was used to extend the time-domain data in all indirectly detected dimensions by 33% (Olejniczak & Eaton, 1990; Press et al., 1992); zero-filling was applied to all dimensions. Linear prediction, Fourier transformation, and base-line corrections of all spectra were carried out on an IRIS Silicon Graphics workstation using the TRITON software package developed in our laboratory. The analysis of all spectra was simplified using the program ALISON (Kleywegt et al., 1993).

RESULTS AND DISCUSSION

Assignment Strategy for the Backbone Nuclei. The analysis started with the determination of NH−^{15}N correlations observed in a high resolution 2D (^{15}N)-HSQC spectrum. Spectral overlap occurred when two amides had ^{15}N chemical shifts that differed by less than 0.2 ppm and NH shifts that differed by less than 0.02 ppm. For the 90 residue HUBst 80 NH−^{15}N backbone correlations were found in the 2D (^{15}N)-HSQC spectrum. Since HUBst contains four prolines (e.g., Pro-63, Pro-72, Pro-77, and Pro-81) and since the amide proton of Met-1 may be unobservable due to solvent exchange, only five (NH,^{15}N) cross-peaks were lacking due to overlap. The good spread of intraresidue NH−^{15}N backbone correlations allowed for a straightforward approach for the sequential backbone assignment using 3D heteronuclear triple-resonance spectra with a completely (^{13}C,^{15}N)-labeled protein.

For the sequential assignment, NH(i) and ^{15}N(i) chemical shifts for each residue i were correlated with the intraresidue backbone resonances ^{13}CO(i), ^{13}C$^{\alpha}$(i), and ^{1}H$^{\alpha}$(i), and with the backbone resonances of the preceding residue ^{13}CO($i-1$), ^{13}C$^{\alpha}$($i-1$), and ^{1}H$^{\alpha}$($i-1$), as described by Ikura et al.

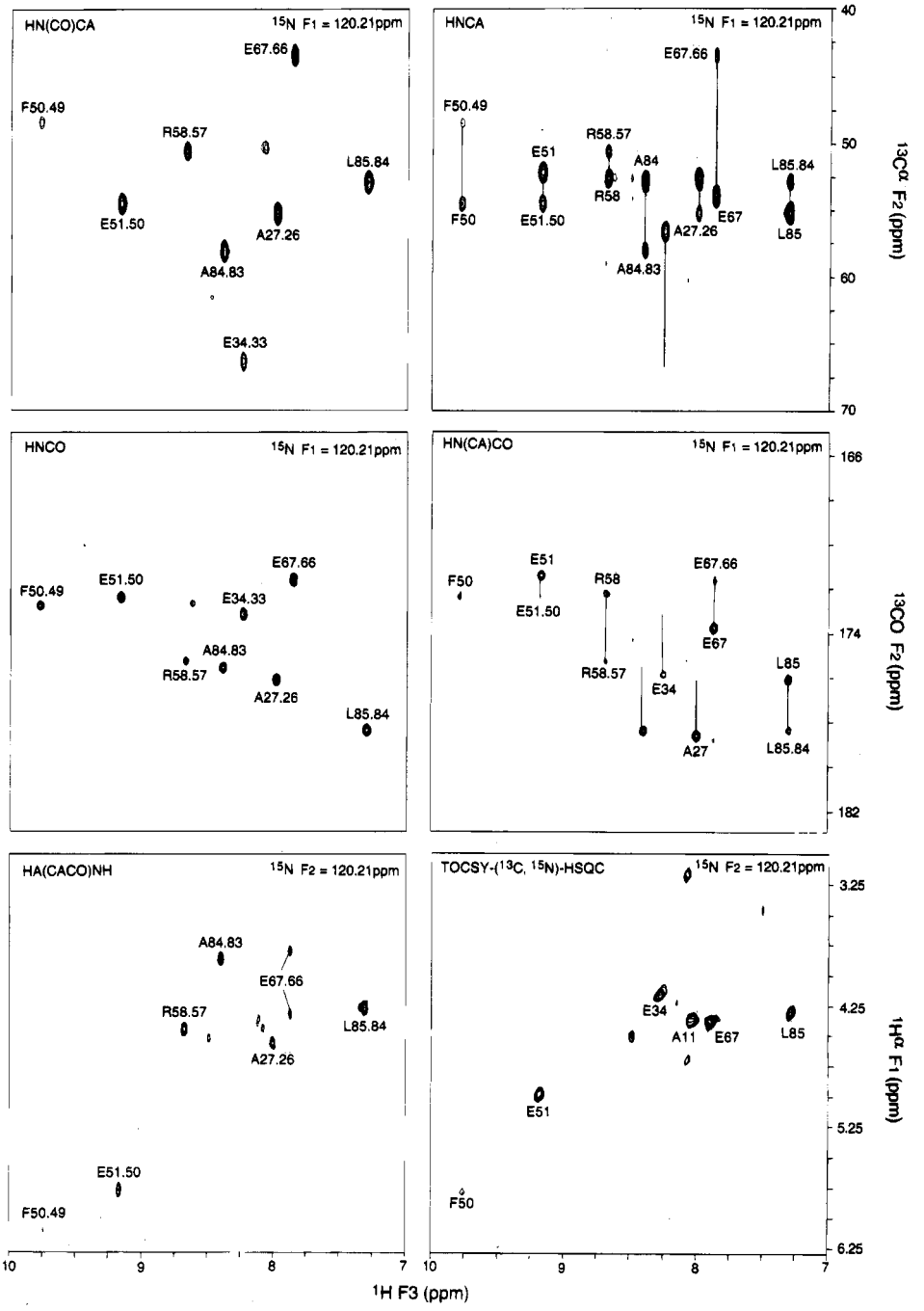

FIGURE 2: Selected $^{13}C^{\alpha}/^{13}CO$ (F_2)$-^1H$ (F_3) planes of the HN(CO)CA, HNCA, HNCO, and HN(CA)CO spectra at a ^{15}N (F_1) chemical shift and ^1H (F_1)$-^1H$ (F_3) planes of the HA(CACO)NH and TOCSY-($^{13}C/^{15}N$)-HSQC spectra at a ^{15}N (F_2) chemical shift of HUBst. The plane at $\delta_{15_N} = 120.21$ ppm represents one of the most crowded in the spectrum.

(1990) and by Clubb et al. (1992). The combined use of different sequential triple-resonance connectivities reduces possibilities of overlap considerably, and therefore ambiguities of sequential connectivities were virtually absent.

The resonances of the sequential and intraresidue $^{13}C^{\alpha}$ backbone nuclei were established from the HN(CO)CA and the HNCA spectra, respectively. The sequential and intraresidue ^{13}CO backbone resonances were established from the HNCO and the HN(CA)CO spectra, respectively. The sequential correlations NH(i)$-$N(i)$-$C$^{\alpha}$($i-1$) and NH(i)$-$N(i)$-$CO($i-1$) measured in the HNCA and the HN(CA)CO spectra, respectively, were merely used as an additional check. The 3D HN(CA)CO experiment was set up in such a way that during the t_2 evolution period pure $^{13}C^{\alpha}-^{13}CO$ multiple quantum coherences evolved. Due to minimal interaction with $^1H^{\alpha}$ spins and due to a minimal number of carbon rf pulses good sensitivity in the HN(CA)CO experiment was obtained. The sequential and intraresidue $^1H^{\alpha}$ resonances were established from the HA(CACO)NH and the TOCSY-(^{13}C,^{15}N)-HSQC spectra, respectively. An example of ^{15}N planes of the six 3D spectra used for the sequential assignment is depicted in Figure 2.

In the next assignment stage linking of adjacent amino acids was accomplished by matching the intraresidue $^{13}C^{\alpha}$, ^{13}CO, and $^1H^{\alpha}$ chemical shifts of residue i with the corresponding sequential $^{13}C^{\alpha}$, ^{13}CO, and $^1H^{\alpha}$ chemical shifts of the adjacent residue ($i + 1$). This appears to be a simple sorting problem. In our case the sorting was accomplished

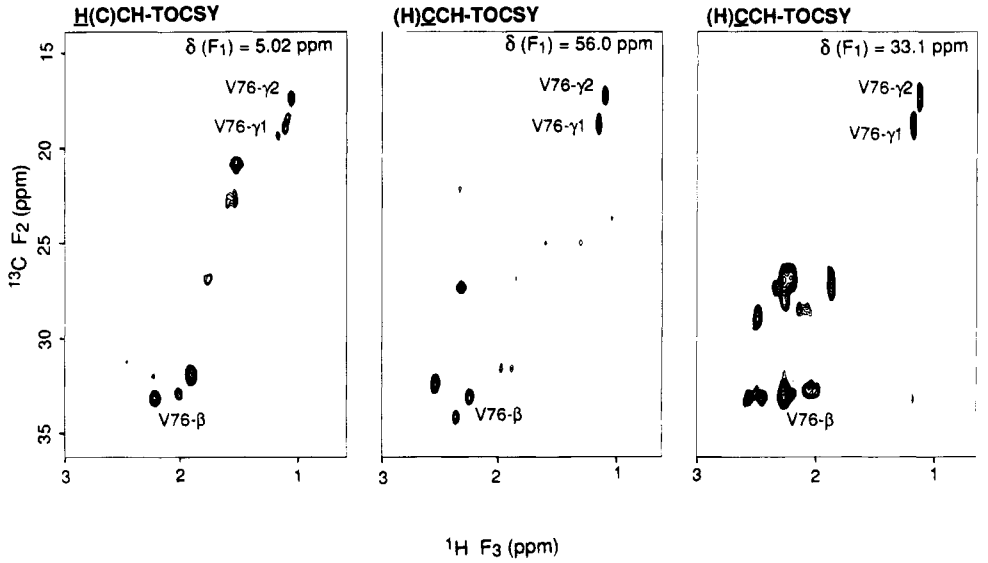

FIGURE 3: F_2-F_3 cross sections from the H(C)CH-TOCSY spectrum at the V76-$^1H^\alpha$ chemical shift and from the (H)CCH-TOCSY spectrum at the V76-$^{13}C^\alpha$ and the V76-$^{13}C^\beta$ chemical shifts. The assignments for this residue are indicated.

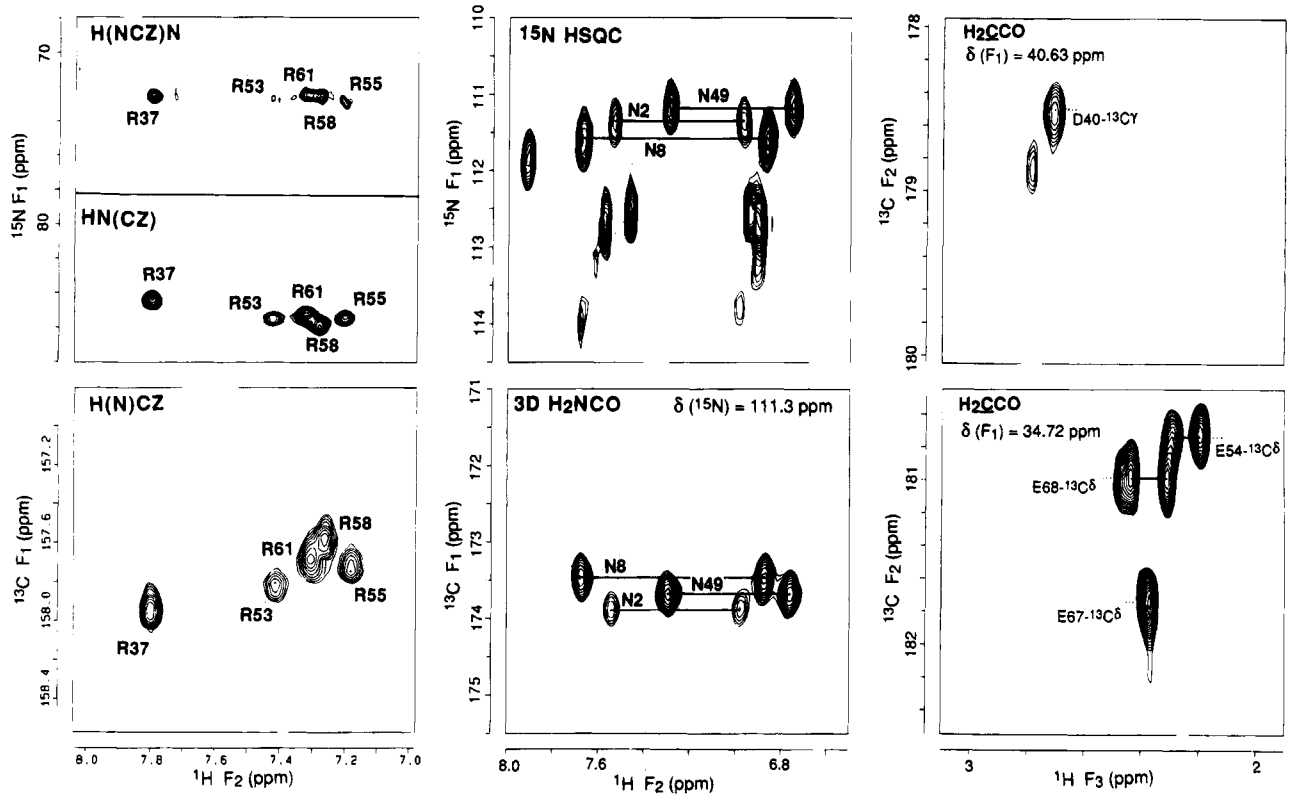

FIGURE 4: Resonance assignments of side chain NH_x and carbonyl nuclei of HUBst. In the 2D HN(CZ), 2D H(N)CZ, and 2D H(NCZ)N spectra the Arg-H^ϵ, Arg-N^ϵ, Arg-C^ζ, and Arg-N^η assignments are indicated. In the 2D (^{15}N)-HSQC side chain NH_2 resonances are observed, and in the F_1-F_3 planes of the 3D H_2NCO and the 3D H_2CCO spectra the side chain carbonyl shifts are correlated to protons of neighboring NH_2 or CH_2 groups, respectively.

by a small computer program, but approaches using commercial database programs, UNIX tools, or visual inspection may be equally useful.

The next requirement comprises the knowledge of some of the linked residue types in order to fit the obtained fragments to the known primary structure. Apart from correlations of amide chemical shifts with the intraresidue $^1H^\alpha$ resonances, correlations of the intraresidue $^1H^\beta$ and of some of the $^1H^\gamma$ proton resonances were observed in the TOCSY-(^{13}C,^{15}N)-HSQC spectrum. The spin systems of alanine, glycine, and valine residues and a number of AMX spin systems were easily identified, while the unambiguous identification of other residues was more cumbersome due to missing signals. The pattern of known residues, however, alternated with well-defined numbers of unknown residue types, matched with unique positions along the backbone. At least five fragments were expected for the whole backbone, separated by one of the four proline residues. For a few residues linking was not immediately obvious. Since the possibilities were limited by only a few unoccupied positions along the backbone, these residues were also assigned unambiguously. The assignment of $^{13}C^\alpha$, ^{13}CO, and

$^1H^\alpha$ backbone chemical shifts was completed by inserting sequential ^{13}CO and $^1H^\alpha$ chemical shifts for the missing intraresidue chemical shifts. The HCACO spectrum, in which the resonances of intraresidue $^1H^\alpha$, $^{13}C^\alpha$, and ^{13}CO nuclei were correlated, was used as an additional check. The HCA(CO)N spectrum, in which correlations were observed between resonances of attached $^1H^\alpha$ and $^{13}C^\alpha$ nuclei and backbone ^{15}N nuclei of the next residues, was used to assign the missing backbone ^{15}N chemical shifts of proline residues and to confirm the sequential backbone resonance assignments.

Assignment Strategy for Side Chain Aliphatic Nuclei. The ^{13}C and ^1H chemical shifts of aliphatic side chains were assigned using the three-dimensional HC(C)H-COSY, H(C)-CH-TOCSY, (H)CCH-TOCSY, and HC(C)H-TOCSY spectra. As the complete backbone assignment had provided the $^{13}C^\alpha$ and $^1H^\alpha$ chemical shifts for each individual residue, these shifts were used as starting points for analysis of these spectra.

The HC(C)H-COSY and HC(C)H-TOCSY spectra were used to read out the ^1H chemical shifts of the side chains in the F_3 direction with a high resolution. The (H)CCH-TOCSY spectrum was used to read out the side chain ^{13}C chemical shifts in the F_1 direction. A procedure for correlating ^{13}C chemical shifts with directly attached ^1H chemical shifts was followed using the (H)CCH-TOCSY and H(C)CH-TOCSY spectra. Correlations of attached carbons and protons are observed as cross-peaks in the ^{13}C (F_2)$-^1H$ (F_3) planes of both spectra, selected at known, though not necessarily assigned, ^{13}C or ^1H chemical shifts in the F_1 direction in the (H)CCH-TOCSY and H(C)CH-TOCSY spectra, respectively. For any choice of ^{13}C or ^1H within one residue it is expected to observe cross-peaks from all the attached $^{13}C-^1H$ pairs of this residue in the selected F_2-F_3 planes of the corresponding spectrum. Each newly assigned resonance was used to check for the existence of the expected cross-peaks. This procedure is demonstrated for Val-76 in Figure 3, in which planes are selected at the $^1H^\alpha$, $^{13}C^\alpha$, and $^{13}C^\beta$ chemical shifts in the F_1 direction of the H(C)CH-TOCSY spectrum and of the (H)CCH-TOCSY spectrum, respectively.

The $C^\epsilon H_3$ chemical shifts of Met-1 and Met-69 were identified using a 2D (^{13}C)-HSQC spectrum and correlated with the $^1H^\gamma$ shifts using ^1H (F_1)$-^1H$ (F_3) cross sections of the NOESY-(^{13}C,^{15}N)-HSQC spectrum selected at the Met-$^{13}C^\epsilon$ chemical shifts in the F_2 (^{13}C) dimension.

All aliphatic ^{13}C shifts were in good agreement with those observed for other proteins, in particular, interleukin-1β (Clore et al., 1990), III^{Glc} from *E. coli* (Pelton et al., 1991), human interleukin-4 (Powers et al., 1992), and ribonuclease H from *E. coli* (Yamazaki et al., 1993). The 3D HC(C)H-COSY and 3D HCCH-TOCSY experiments have provided nearly complete ^{13}C and ^1H resonance assignments of the aliphatic side chain nuclei of HUBst, except for those of Lys-3, Lys-18, and Lys-86. For Lys-3, correlations were only observed for the $C^\beta H_2$ and $C^\gamma H_2$ groups in the 3D HCCH-COSY and the NOESY-(^{13}C,^{15}N)-HSQC spectra. The $^{13}C^\alpha H$ and the $^1H^\beta$ chemical shifts of Lys-18 and Lys-86 are identical, and therefore, side chain resonances CH_2 groups could not be assigned unambiguously.

Side Chain Aromatic Nuclei Assignments. Chemical shift correlations between aromatic ring carbons and the directly attached protons were obtained from the 2D (^{13}C)-HSQC

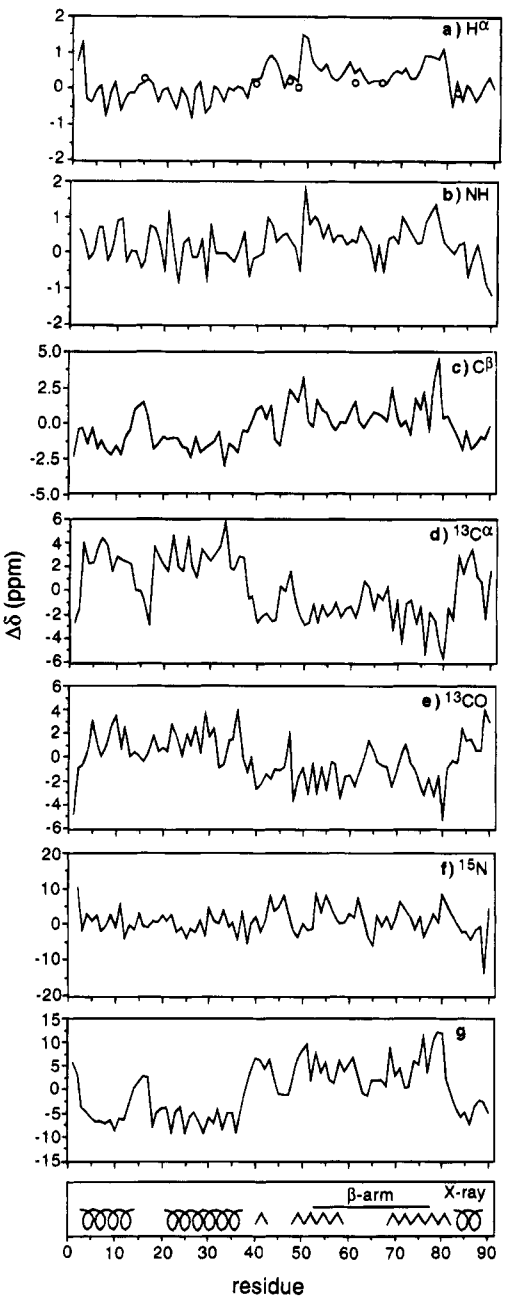

FIGURE 5: Mapping of $^1H^\alpha$, $^1H^N$, $^{13}C^\beta$, $^{13}C^\alpha$, ^{13}CO, and ^{15}N chemical shifts (a–f) relative to the random coil value along the amino acid sequence for a monomer of HUBst. (○) indicates the values for second glycine α-protons. For $^1H^\alpha$, $^{13}C^\alpha$, ^{13}CO, and $^{13}C^\beta$ chemical shifts and for the combination $\Delta\delta_{^1H^\alpha} - \Delta\delta_{^{13}CO} - \Delta\delta_{^{13}C^\alpha} + \Delta\delta_{^{13}C^\beta}$ (g) a good correlation exists with the secondary structure observed in the X-ray structure.

spectrum. A search through the ^1H (F_2)$-^1H$ (F_3) planes of the aromatic 3D (^{13}C)-HSQC-TOCSY spectrum at these ^{13}C chemical shifts in the F_1 direction was executed to identify the spin systems of the four phenylalanine aromatic ring protons. The ^1H resonances that were correlated with two other aromatic ^1H chemical shifts were assigned to $^1H^\epsilon$ protons. The usually lower Phe-$^{13}C^\zeta$ shifts relative to Phe-$^{13}C^\delta$ shifts (Clore et al., 1990; Powers et al., 1992; Yamazaki et al., 1993) and the doubled intensities observed for overlapping $^1H^\delta$ signals relative to $^1H^\zeta$ signals resonances helped to distinguish between the $C^\delta H$ and $C^\zeta H$ correlations observed in the (^{13}C)-HSQC spectrum. The linkages of the aromatic chemical shifts with the backbone were accomplished by NOE data obtained from a 3D time-shared

NOESY-(^{13}C,^{15}N)-HSQC spectrum; ^{1}H (F_1)−^{1}H (F_3) planes were selected at the $^{13}C^{\beta}$ and the $^{13}C^{\alpha}$ chemical shift, in which strong intraresidue NOE signals were observed between the $^1H^{\beta}$ and $^1H^{\delta}$ shifts and medium intraresidue NOE signals between $^1H^{\alpha}$ and $^1H^{\delta}$, respectively.

Exchange broadening of the aromatic ring proton signals of Phe-79 was observed in the 2D (^{13}C)-HSQC spectrum at 311 K. Increasing the temperature resulted in sharpening of these lines without any change of chemical shifts, indicating that the aromatic ring rotation of Phe-79 at 311 K is in the fast-exchange region. However, at 299 K these signals vanished completely, while three other aromatic CH correlations appeared in the 2D (^{13}C)-HSQC spectrum at $\delta\{^1H/^{13}C\}$ = 7.48 ppm/130.4 ppm, $\delta\{^1H/^{13}C\}$ = 7.37 ppm/129.4 ppm, and $\delta\{^1H/^{13}C\}$ =7.43 ppm/127.7 ppm. Apparently, Phe-79 shows an exchange between different environments.

Side Chain Amide Nitrogen and Hydrogen Assignments. From the 2D (^{15}N)-HSQC spectrum six pairs of signals, sharing the ^{15}N chemical shift, were observed originating from the $N^{\delta}H_2$ and $N^{\epsilon}H_2$ nuclei of four asparagine and two glutamine residues. The chemical shifts of the NH_2 groups were specifically assigned using the 3D time-shared NOESY-(^{13}C,^{15}N)-HSQC spectrum. The NOE correlations from $^1H^{\beta}$ and $^1H^{\gamma}$ chemical shifts to $^1H^{\delta}$ and $^1H^{\epsilon}$ chemical shifts were observed in the F_1-F_3 planes selected at the Asn-$^{15}N^{\delta}$ and the Gln-$^{15}N^{\epsilon}$ chemical shifts, respectively. The delay for the magnetization transfer from proton to nitrogen and vice versa in the HN(CO)CA experiment allowed the detection of NH_2 proton chemical shifts, modulated with the attached ^{15}N chemical shift in t_1 and with the Asn-$^{13}C^{\beta}$ or the Gln-$^{13}C^{\gamma}$ chemical shift in t_2. Weak correlations observed in the HN-(CO)CA confirmed the assignments of the NH_2 chemical shifts.

From the 2D HN(CZ), the 2D H(N)CZ, and the 2D H(NCZ)N spectra the Arg-$^{15}N^{\epsilon}$, Arg-$^{13}C^{\zeta}$, and Arg-$^{15}N^{\eta}$ chemical shifts were correlated with the Arg-$^1H^{\epsilon}$ chemical shifts, respectively. The relevant parts of these spectra are shown in Figure 4. Subsequently, the 3D TOCSY-(^{13}C,^{15}N)-HSQC spectrum was used to correlate the four grouped chemical shifts of arginine residues with the correct residue in the amino acid sequence; F_1−F_3 planes were selected at the Arg-$^{15}N^{\epsilon}$ chemical shifts, in which the $^1H^{\epsilon}$ chemical shift in the F_3 dimension was correlated with other aliphatic side chain chemical shifts in the F_1 dimension. Since the Arg-$^{15}N^{\epsilon}$ nuclei have chemical shifts at about 85 ppm, the correlations were observed as folded and inverted signals, compared to the signals near the carrier frequency.

In the 2D H(C)N spectrum correlations were observed between ^{15}N and the attached CH or CH_2 proton chemical shifts. $^{15}N^{\zeta}$ resonances of Lys-59 and Lys-80 were assigned; the remaining Lys-$^{15}N^{\zeta}$ chemical shifts were about 33.9 ppm and could not be assigned unambiguously due to the overlap of Lys-$^1H^{\epsilon}$ resonances. The ^{15}N resonance of Met-1 was not observed in the 2D H(C)N spectrum and is therefore not assigned. Since the Arg-$^1H^{\eta}$ nuclei are in fast exchange with water, the $N^{\eta}H_2$ correlations in the (^{15}N)-HSQC spectrum were broadened and weak. Arg-$^1H^{\eta}$ signals appeared at 7.0 and 6.7 ppm, but the low dispersion in chemical shifts of the attached nitrogens prevented unambiguous discrimination of the $N^{\eta}H_2$ correlations. $N^{\zeta}H$ correlations of lysines were not observed in the (^{15}N)-HSQC spectrum; also for lysines the low dispersion in $^{15}N^{\zeta}$ chemical shifts would make it difficult to observe directly unambiguous $N^{\zeta}H$ correlations.

Side Chain Carboxyl and Carbonyl Carbon Assignments. The carboxyl carbon resonances Asn-$^{13}C^{\gamma}$ and Gln-$^{13}C^{\delta}$ were correlated with the ^{15}N and ^{1}H chemical shifts of the Asn-$N^{\delta}H_2$ nuclei and the Gln-$N^{\epsilon}H_2$ nuclei using the 3D H_2NCO spectrum. The ^{13}CO chemical shifts were identified along the two proton chemical shifts of the concerning NH_2 groups observed in the F_2 (^{13}CO)−F_3 (^{1}H) cross sections selected at the ^{15}N chemical shifts in the F_1 direction. A plane at $\delta(^{15}N)$ = 111.34 ppm is shown in Figure 4.

The carbonyl carbon resonances Asp-$^{13}C^{\gamma}$ and Glu-$^{13}C^{\delta}$ were assigned from the H_2CCO spectrum, in which they were correlated with the two neighboring methylene Asp-$^1H^{\beta}$ and Glu-$^1H^{\gamma}$ chemical shifts in F_2 (^{13}CO)−F_3 (^{1}H) planes selected at the methylene ^{13}C chemical shifts in the F_1 direction. Similarly, the H_2CCO spectrum was used to confirm the assignments of all Asn-$^{13}C^{\gamma}$, Gln-$^{13}C^{\delta}$, and Gly-^{13}CO chemical shifts, which were correlated with adjacent $C^{\beta}H_2$, $C^{\gamma}H_2$, and $C^{\alpha}H_2$ chemical shifts, respectively. Two examples of ^{13}CO−^{1}H planes in the H_2CCO spectrum at $\delta(^{13}C)$ = 40.63 ppm and at $\delta(^{13}C)$ = 34.72 ppm are presented in Figure 4.

The complete list of ^{1}H, ^{13}C, and ^{15}N resonance assignments of HUBst is presented in Table 1.

Secondary Structure Analysis Using Chemical Shifts. Wishart et al. (1991, 1994) have shown that ^{1}H, ^{13}C, and ^{15}N chemical shifts can be used for qualitative identification of secondary structure elements in proteins. A mapping of $^1H^{\alpha}$, NH, $^{13}C^{\beta}$, $^{13}C^{\alpha}$, ^{13}CO, and ^{15}N chemical shifts relative to the random coil value along the primary sequence of HUBst is shown in the Figure 5, panels a−f, respectively, together with the positions of secondary structure elements, as found in the X-ray structure. An upfield shift of α-proton, amide proton, and β-carbon resonances and a downfield shift of α-carbon and backbone carbonyl carbon resonances are strong indications of an α-helix. By contrast, a β-sheet is indicated by a downfield shift of α-proton, amide proton, and β-carbon resonances and an upfield shift of α-carbon and backbone carbonyl carbon resonances (Pardi et al., 1983; Spera & Bax, 1991; Wishart et al., 1991, 1994). Similar trends are indeed observed in Figure 5 and are in good agreement with the secondary structure deduced from the X-ray structure, with the exception of the backbone NH chemical shifts in the first two helices, which show a rather scattered distribution around the random coil value. A poor correlation between backbone NH shifts and secondary structure was also noted by Wishart et al. (1994). Also for backbone nitrogen chemical shifts no correlation was found with the presence of ordered secondary structure elements.

Flexible parts of the molecule are expected to have chemical shifts closer to the random coil values, and accordingly our chemical shift data are consistent with the positions of the three turns connecting the secondary structure elements. Particularly noteworthy are the $^1H^{\alpha}$ chemical shifts of the successive residues 57−61 in the β-arm, which all adopt the random coil value. It is also of note that the backbone chemical shifts in the N-terminal region differ substantially from the random coil value, which suggests that this part is structured.

Moreover, the cumulative effect of $^1H^{\alpha}$, $^{13}C^{\alpha}$, $^{13}C^{\beta}$, and ^{13}CO chemical shifts relative to the random coil value (presented in Figure 5g) shows even more consistency with the anticipated secondary structure. The good agreement of

Table 1: Chemical Shifts (ppm) of ^{1}H, ^{13}C, and ^{15}N Nuclei in HU from *B. stearothermophilus*[a]

residue	^{15}N	C=O	C^{α}	C^{β}	others
M1		169.8	53.0 (5.07)	28.8 (2.14, 2.14)	C^{γ} 32.2 (2.36, 2.25)
					C^{ϵ} 15.9 (2.15)
N2	129.2 (8.97)	173.7	49.0 (5.94)	37.4 (3.69, 3.21)	C^{γ} 173.9
					N^{δ} 111.4 (7.57, 7.01)
K3	119.6 (8.70)	175.5	59.2 (3.95)	31.3 (2.24, 2.11)	C^{γ} 23.8 (1.70)
T4	116.2 (7.98)	174.3	65.1 (3.99)	66.9 (4.37)	C^{γ} 20.0 (1.38)
E5	122.2 (8.43)	177.7	57.3 (4.19)	28.3 (2.18, 2.18)	C^{γ} 35.0 (2.67, 2.49)
					C^{δ} 181.2
L6	124.7 (8.72)	175.9	56.6 (4.44)	39.2 (2.36, 1.65)	C^{γ} 25.7 (1.07)
					C^{δ} 22.1 (1.16)
					C^{δ} 22.1 (1.16)
I7	121.1 (8.69)	175.5	64.8 (3.44)	35.8 (2.14)	$C^{\gamma 1}$ 29.1 (2.04, 0.94)
					$C^{\gamma 2}$ 15.8 (0.99)
					C^{δ} (13.3 (1.14)
N8	118.7 (8.10)	175.6	54.4 (4.47)	35.8 (3.00, 3.00)	C^{γ} 173.5
					N^{δ} 111.6 (7.69, 6.89)
A9	124.9 (8.22)	178.7	53.3 (4.38)	15.7 (1.69)	
V10	121.3 (8.97)	177.7	64.3 (3.51)	29.4 (2.34)	C^{γ} 21.8 (0.99)
					C^{γ} 18.0 (0.91)
A11	127.8 (9.08)	176.8	54.3 (3.92)	15.6 (1.54)	
E12	117.3 (8.14)	177.2	57.4 (4.13)	27.8 (2.30, 2.23)	C^{γ} 33.8 (2.50, 2.45)
					C^{δ} 182.2
T13	113.0 (8.23)	173.8	63.3 (4.24)	67.7 (4.21)	C^{γ} 20.0 (1.41)
S14	114.9 (8.33)	172.8	58.1 (4.46)	63.3 (3.87, 3.73)	
G15	112.0 (7.93)	172.2	43.9 (4.27, 3.96)		
L16	121.8 (7.75)	174.5	51.9 (4.62)	42.5 (1.72, 1.48)	C^{γ} 25.0 (1.70)
					C^{δ} 20.8 (0.92)
					C^{δ} 23.2 (0.76)
S17	115.8 (9.06)	172.8	55.2 (4.49)	62.5 (4.48, 4.25)	
K18	122.5 (8.97)	178.0	58.9 (3.89)	29.8 (2.01, 1.97)	C^{γ} 23.9 (1.63, 1.47)
					C^{δ} 27.1 (1.83)
					C^{ϵ} 40.0 (3.14)
K19	121.9 (8.56)	176.7	58.0 (4.17)	30.2 (2.00, 1.87)	C^{γ} 22.6 (1.66, 1.53)
					C^{δ} 27.0 (1.85)
					C^{ϵ} 40.2 (3.14)
D20	122.6 (7.85)	176.1	55.5 (4.66)	38.6 (2.89, 2.57)	C^{γ} 175.9
A21	123.1 (9.27)	176.6	53.3 (3.88)	16.7 (1.45)	
T22	115.9 (8.26)	176.6	65.6 (3.79)	67.1 (4.56)	C^{γ} 18.5 (1.34)
K23	119.2 (7.43)	177.8	57.2 (4.23)	30.6 (2.15, 1.88)	C^{γ} 22.9 (1.73)
					C^{δ} 27.5 (1.95)
					C^{ϵ} 40.3 (3.16)
A24	121.3 (8.38)	176.1	53.3 (3.95)	16.2 (1.28)	
V25	118.4 (8.48)	176.1	65.9 (3.28)	29.3 (2.19)	C^{γ} 22.4 (1.07)
					C^{γ} 19.5 (1.01)
D26	118.7 (8.25)	176.3	55.5 (4.61)	37.2 (2.76, 2.76)	C^{γ} 176.4
A27	120.1 (8.00)	178.7	52.8 (4.38)	17.0 (1.65)	
V28	123.4 (8.45)	174.6	65.1 (3.33)	29.1 (2.00)	C^{γ} 22.9 (1.00)
					C^{γ} 19.3 (0.16)
F29	117.1 (7.13)	177.2	60.4 (3.90)	35.3 (2.95, 2.88)	C^{δ} 129.6 (6.41)
					C^{ϵ} 127.7 (6.70)
					C^{ζ} 126.8 (6.59)
D30	124.6 (9.16)	177.0	55.8 (4.67)	38.1 (2.91, 2.82)	C^{γ} 176.5
S31	117.4 (8.28)	174.8	61.2 (4.34)	61.0 (4.12, 3.67)	
I32	123.1 (7.97)	174.6	64.3 (3.71)	36.4 (1.83)	$C^{\gamma 1}$ 27.3 (0.84)
					$C^{\gamma 2}$ 14.2 (0.66)
					C^{δ} 11.3 (0.57)
T33	117.2 (8.14)	173.2	66.8 (4.39)	65.1 (3.99)	C^{γ} 20.1 (1.37)
E34	120.4 (8.25)	176.0	56.8 (4.18)	27.3 (2.22, 2.17)	C^{γ} 33.3 (2.55, 2.43)
					C^{δ} 181.3
A35	122.6 (7.86)	177.6	53.4 (4.24)	16.4 (1.56)	
L36	117.8 (8.06)	178.9	55.7 (4.38)	39.1 (2.00, 1.39)	C^{γ} 24.9 (2.14)
					C^{δ} 20.3 (1.03)
					C^{δ} 24.1 (0.96)
R37	123.2 (8.82)	175.9	57.8 (4.05)	28.6 (2.11, 2.11)	C^{γ} 25.0 (1.75)
					C^{δ} 41.8 (3.40)
					N^{ϵ} 84.8 (7.80)
					C^{ζ} 158.0
					N^{η} 72.7
K38	116.2 (7.60)	174.9	54.5 (4.48)	30.5 (2.14, 2.14)	C^{γ} 22.6 (1.58)
					C^{δ} 27.1 (1.83)
					C^{ϵ} 40.3 (3.15)
G39	109.3 (8.17)	172.2	43.5 (4.37, 3.82)		
D40	122.4 (8.31)	172.6	50.8 (4.94)	40.5 (2.72, 2.72)	C^{γ} 178.7

Table 1 (Continued)

residue	^{15}N	C=O	C^{α}	C^{β}	others
K41	119.3 (8.28)	174.0	53.1 (4.93)	32.9 (1.98, 1.93)	C^{γ} 23.0 (1.67, 1.57) C^{δ} 27.7 (1.82) C^{ϵ} 40.3 (3.12)
V42	123.9 (9.08)	172.8	59.6 (5.02)	31.2 (2.48)	C^{γ} 19.5 (1.15) C^{γ} 18.7 (1.06)
Q43	128.9 (8.95)	172.3	52.9 (5.05)	28.9 (2.14, 2.14)	C^{γ} 32.2 (2.36, 2.25) C^{δ} 178.4 N^{ϵ} 112.6 (7.49, 6.97)
L44	126.0 (8.30)	173.9	50.4 (4.89)	39.9 (2.57, 1.22)	C^{γ} 24.3 (1.66) C^{δ} 21.0 (0.70) C^{δ} 24.0 (0.61)
I45	128.1 (8.47)	174.4	61.1 (4.11)	35.5 (2.09)	$C^{\gamma 1}$ 26.3 (1.73, 1.45) $C^{\gamma 2}$ 15.1 (1.14) C^{δ} 11.2 (1.10)
G46	117.5 (8.91)	171.3	43.9 (4.49, 3.86)		
F47	122.4 (8.23)	175.5	59.1 (4.70)	39.2 (2.96, 2.70)	C^{δ} 130.3 (7.26) C^{ϵ} 129.8 (7.18) C^{ζ} 126.8 (6.52)
G48	107.5 (8.50)	168.4	43.6 (4.30, 3.69)		
N49	115.3 (7.83)	172.9	48.7 (6.15)	39.2 (2.77, 2.57)	C^{γ} 173.7 N^{δ} 111.2 (7.33, 6.79)
F50	120.6 (9.79)	172.5	54.7 (5.83)	40.5 (3.24, 3.17)	C^{δ} 130.4 (7.23) C^{ϵ} 129.0 (6.74) C^{ζ} 126.7 (7.20)
E51	119.9 (9.18)	171.5	52.4 (5.00)	31.8 (2.24, 2.11)	C^{γ} 33.0 (2.02) C^{δ} 180.7
V52	121.1 (9.12)	173.7	60.2 (4.69)	30.7 (2.17)	C^{γ} 20.9 (1.17) C^{γ} 20.3 (0.99)
R53	128.4 (9.11)	172.8	52.4 (4.83)	30.5 (1.97, 1.79)	C^{γ} 25.0 (1.67) C^{δ} 41.3 (3.27) N^{ϵ} 85.8 (7.41) C^{ζ} 157.9 N^{η} 72.8
E54	124.7 (8.80)	173.8	53.7 (4.92)	29.3 (2.14, 2.03)	C^{γ} 34.4 (2.31, 2.22) C^{δ} 180.8
R55	127.7 (9.02)	173.1	52.9 (4.66)	29.6 (1.99, 1.85)	C^{γ} 24.9 (1.76) C^{δ} 41.8 (3.31) N^{ϵ} 85.7 (7.18) C^{ζ} 157.7 N^{η} 72.9
A56	127.4 (8.40)	175.7	50.0 (4.43)	17.7 (1.57)	
A57	124.3 (8.59)	175.5	50.7 (4.50)	17.5 (1.53)	
R58	119.7 (8.69)	172.4	52.9 (4.84)	31.2 (1.98, 1.89)	C^{γ} 24.5 (1.74, 1.61) C^{δ} 41.8 (3.32) N^{ϵ} 86.7 (7.26) C^{ζ} 157.7 N^{η} 72.7
K59	121.9 (8.51)	174.6	53.7 (4.99)	31.7 (1.91, 1.91)	C^{γ} 22.8 (1.59, 1.53) C^{δ} 26.9 (1.76) C^{ϵ} 40.2 (3.09) N^{ζ} 33.7
G60	112.0 (8.72)	170.6	42.7 (4.54, 3.85)		
R61	121.4 (8.51)	173.4	52.8 (4.89)	30.6 (1.74, 1.65)	C^{γ} 25.2 (1.58, 1.48) C^{δ} 41.3 (3.25) N^{ϵ} 85.6 (7.31) C^{ζ} 157.8 N^{η} 72.6
N62	126.5 (9.09)	173.2	49.3 (5.00)	37.7 (3.27, 2.87)	C^{γ} 175.2 N^{δ} 116.2 (7.75, 7.43)
P63	126.8	174.4	62.5 (4.49)	30.2 (2.49, 2.49)	C^{γ} 25.2 (2.21, 2.15) C^{δ} 49.0 (4.20, 3.96)
Q64	116.9 (8.41)	175.5	55.8 (4.50)	27.8 (2.32, 2.32)	C^{γ} 32.7 (2.54) N^{ϵ} 112.8 (7.60, 6.92)
T65	107.2 (7.65)	174.4	59.4 (4.60)	69.0 (4.52)	C^{γ} 19.3 (1.28)
G66	111.8 (8.59)	171.7	43.7 (4.35, 3.83)		
E67	120.7 (7.87)	173.9	54.2 (4.41)	29.3 (2.20, 1.99)	C^{γ} 34.3 (2.39) C^{δ} 181.8
E68	123.5 (8.81)	173.7	55.3 (4.65)	28.6 (2.11, 2.11)	C^{γ} 34.8 (2.46, 2.33) C^{δ} 181.1
M69	123.0 (8.59)	172.0	52.4 (4.84)	33.7 (2.06, 2.06)	C^{γ} 29.1 (2.48) C^{ϵ} 15.2 (2.18)
E70	123.6 (8.66)	173.4	54.1 (4.69)	29.0 (2.10, 2.02)	C^{γ} 33.9 (2.29, 2.20) C^{δ} 181.8

Table 1 (Continued)

residue	^{15}N	C=O	C^{α}	C^{β}	others
I71	129.6 (9.02)	175.5	56.3 (4.65)	36.7 (1.98)	$C^{\gamma 1}$ 25.3 (1.56, 1.25)
					$C^{\gamma 2}$ 15.1 (1.09)
					C^{δ} 10.8 (0.91)
P72	129.9	175.7	60.6 (4.61)	30.8 (2.49, 2.49)	C^{γ} 25.2 (2.12)
					C^{δ} 49.3 (4.04, 3.85)
A73	124.3 (8.60)	175.6	50.6 (4.48)	17.4 (1.57)	
S74	115.0 (8.56)	171.2	55.4 (4.87)	64.1 (3.96, 3.89)	
K75	123.7 (8.58)	173.9	53.9 (5.14)	32.7 (1.89, 1.62)	C^{γ} 23.4 (1.60, 1.39)
					C^{δ} 27.4 (1.83)
					C^{ϵ} 40.2 (3.13)
V76	118.8 (8.94)	171.0	56.1 (5.02)	33.2 (2.23)	C^{γ} 19.2 (1.09)
					C^{γ} 17.7 (1.03)
P77	130.7	173.0	59.9 (5.20)	29.9 (2.29, 1.99)	C^{γ} 25.4 (2.10, 2.00)
					C^{δ} 48.2 (4.12, 3.81)
A78	125.3 (9.48)	172.8	49.3 (5.02)	21.1 (1.51)	
F79	120.8 (8.64)	171.9	52.6 (5.54)	41.7 (2.93, 2.63)	C^{δ} 130.3 (6.24)
					C^{ϵ} 127.6 (6.57)
					C^{ζ} 128.4 (6.38)
K80	130.1 (8.58)	170.9	49.5 (4.77)	32.0 (1.68, 1.55)	C^{γ} 22.1 (1.40, 1.27)
					C^{δ} 27.1 (1.71)
					C^{ϵ} 40.1 (3.02)
					N^{ζ} 34.1
P81	130.6	173.7	60.4 (3.87)	31.1 (1.92, 1.92)	C^{γ} 24.9 (2.11)
					C^{δ} 49.0 (3.92, 3.58)
G82	111.8 (8.34)	171.8	41.5 (4.32, 3.55)		
K83	121.7 (8.52)	175.7	58.2 (3.89)	30.7 (2.03, 1.94)	C^{γ} 22.6 (1.58, 1.54)
					C^{δ} 27.0 (1.86, 1.75)
					C^{ϵ} 40.4 (3.17)
A84	119.9 (8.41)	178.5	53.1 (4.31)	15.9 (1.55)	
L85	120.2 (7.31)	176.3	55.5 (4.33)	40.4 (1.86, 1.73)	C^{γ} 22.2 (1.12)
					C^{δ} 23.9 (0.66)
					C^{δ} 23.9 (0.66)
K86	117.3 (8.12)	177.7	58.8 (3.89)	29.8 (2.02, 1.97)	C^{γ} 23.9 (1.63, 1.47)
					C^{δ} 27.3 (1.83)
					C^{ϵ} 40.0 (3.14)
D87	118.6 (8.60)	175.9	54.7 (4.52)	38.2 (2.88, 2.76)	C^{γ} 177.1
A88	121.6 (7.77)	176.7	52.4 (4.35)	17.0 (1.65)	
V89	108.4 (7.16)	178.2	59.1 (4.43)	29.9 (2.47)	C^{γ} 17.5 (0.97)
					C^{γ} 19.8 (0.95)
K90	125.9 (7.13)	179.2	56.8 (4.26)	31.5 (2.02, 2.02)	C^{γ} 22.6 (1.69)
					C^{δ} 27.9 (1.90)
					C^{ϵ} 40.5 (3.20)

[a] Solution conditions: 2.2 mM HU, 200 mM potassium chloride, and 50 mM phosphate in a mixture of 95% H_2O/5% D_2O at pH 4.6 and at 311 K. ^1H chemical shifts of protons attached to the assigned heteronucleus are indicated in parentheses. The accuracy (ppm) of the ^1H, ^{13}C, and ^{15}N chemical shifts are 0.04, 0.2, and 0.2, respectively. The ^1H chemical shifts are relative to internal TSP. The ^{13}C chemical shifts are relative to the methyl signal of TMS. The ^{15}N chemical shifts are relative to the $^{15}NH_4Cl$ (acidic) signal.

chemical shift data with the secondary structure obtained from crystallographic data is a confirmation of the assignment of backbone chemical shifts.

Secondary Structure Analysis from NOE Data and Fast Exchanging Amide Protons. Sequential and medium and long range NOEs have been collected using a NOESY-(^{13}C,^{15}N)-HSQC and a 3D (^{15}N)-HMQC-NOESY-(^{13}C,^{15}N)-HSQC spectrum. In the NOESY-(^{13}C,^{15}N)-HSQC experiment ^{13}C and ^{15}N resonances are modulated simultaneously in the second dimension, allowing for the detection of both aliphatic and amide protons during data acquisition, whereas in the common 3D NOESY-(^{15}N)-HSQC experiment only amide protons are detected. It is shown in Figure 6 that NOEs to NH and $^1H^{\alpha}$ of Ile-45 in particular can be assigned in different planes of one NOESY-(^{13}C,^{15}N)-HSQC spectrum. Also, the equivalent $^1H^{\alpha}$ cross section of the TOCSY-(^{13}C,^{15}N)-HSQC spectrum is shown to emphasize the quality of the time-shared spectra. The (^{15}N)-HMQC-NOESY-(^{13}C,^{15}N)-HSQC spectrum was used to resolve ambiguities of d_{NN} and $d_{\alpha N}$ NOEs.

The sequential and medium range NOEs and fast exchanging amide protons which were identified for HUBst are shown schematically in Figure 7. Strong sequential d_{NN} NOEs, weak sequential $d_{\alpha N}$ NOEs, and the presence of medium range $d_{NN}(i,i+2)$, $d_{\alpha N}(i,i+3)$, $d_{\alpha N}(i,i+4)$, and $d_{\alpha\beta}(i,i+3)$ NOEs identify the residues which are in an α-helical conformation (Wüthrich, 1986). The combination of strong d_{NN} NOEs and medium range NOEs clearly shows that the first α-helix starts at Lys-3 and extends at least to Thr-13, which is completely in agreement with the X-ray structure, but the presence of a $d_{\alpha N}$ NOE between Ala-11 and Ser-14 can be judged as a continuation of this α-helix to Ser-14. This is supported by a continuous series of slowly exchanging amides ranging from Lys-3 to Ser-14. The presence of a second α-helix is distinctly recognized from Figure 7, but the starting residue of this α-helix is not directly obvious. Strong sequential d_{NN} NOEs are only observed starting from Lys-23, whereas $d_{\alpha N}(i,i+3)$ NOEs are present already starting from Ser-17, $d_{NN}(i,i+2)$ NOEs starting from Lys-18, and $d_{\alpha\beta}(i,i+3)$ NOEs starting from Lys-19. The intensities of sequential d_{NN} NOEs found in the region between Lys-18 and Lys-23 suggest the possibility that the second α-helix starts at Lys-18 and possibly at Ser-17. A series of slowly exchanging amides starting at Ala-21 confirms that Lys-18

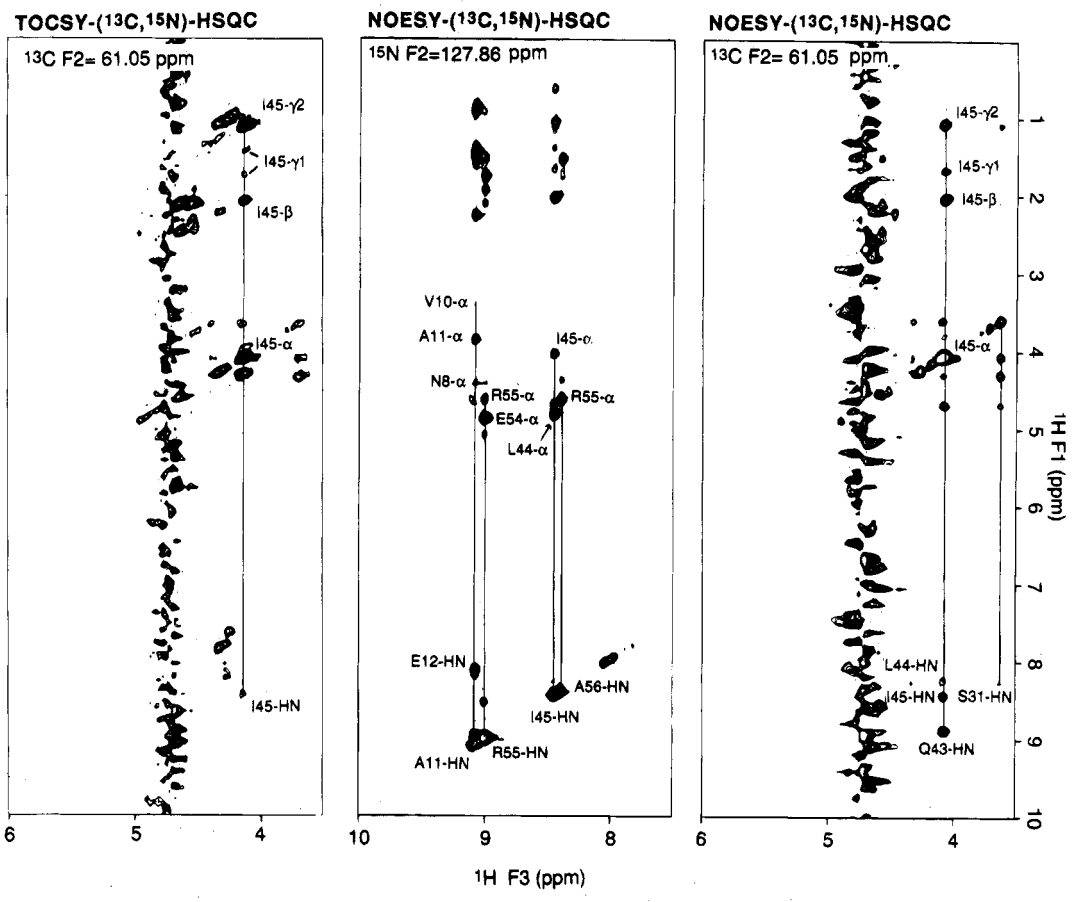

FIGURE 6: Selected ^1H (F_1)−^1H (F_3) planes of the 3D TOCSY-(^{13}C,^{15}N)-HSQC spectrum at $\delta_{^{13}C}$ (F_2) = 61.05 ppm (I45-$^{13}C^{\alpha}$), corresponding with $\delta_{^{13}C}$ (F_2) = 27.88 ppm for the folded spectrum, and of the 3D NOESY-(^{13}C,^{15}N)-HSQC spectrum of HUBst at $\delta_{^{15}N}$ (F_2) = 127.86 ppm (I45-^{15}N) and at $\delta_{^{13}C}$ (F_2) = 61.01 ppm.

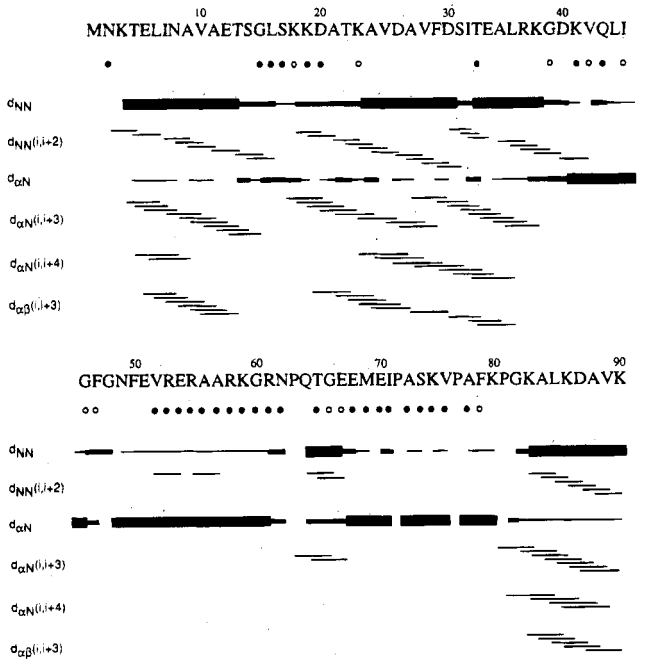

FIGURE 7: Summary of the sequential and medium range NOEs for a monomer of HUBst. The thickness of the lines for the sequential NOEs correlates with the intensity of the NOE. The black circles on the first row denote residues that contain fast-exchanging amide protons, and open circles represent the amides that exchange on an intermediate time scale.

can be the first residue of the second α-helix. The second α-helix extends to Arg-37. The chemical shift changes in Figures 5, panels a, c, d, e, and g, also indicate that the second α-helix indeed starts at Lys-18 and extends to Arg-37. A third α-helix is identified starting at Lys-83 and possibly at Gly-82 and extending to Lys-90. The positions of the α-helices are in good agreement with the X-ray structure (White et al., 1989; Wilson, unpublished results).

An extended structure is characterized by strong sequential $d_{\alpha N}$ NOEs and weak d_{NN} NOEs. Three strands with such contacts are recognized. The first strand extends from Asp-40 to Ile-45 and is connected via a turn to the second strand from Gly-48 to Arg-61. The third strand extends from Glu-67 to Lys-80 or Pro-81. The NOE analysis of the secondary structure cannot ascertain whether Pro-81 is included in the third strand. It is noteworthy that Pro-81 is conserved in a few other related proteins, such as IHF-α and IHF-β in *E. coli* and TF1 in *Bacillus subtilis* bacteriophage SPO1 (Drlica et al., 1987). Long range backbone-to-backbone NOEs, characteristic for an antiparallel β-sheet conformation, were observed between the first and the second strand, and between the second and the third strand, as indicated in Figure 8A. Additional support for this arrangement of the three strands is provided by exchange data; the amides of Asp-40, Val-42, Leu-44, Gly-48 to Glu-51, and Lys-80 are involved in putative hydrogen bonds, and those amide protons are in slow exchange with water, as shown in Figure 7. The arrangement of the three strands is the same as in the X-ray structure.

Long range backbone-to-backbone NOEs observed in the β-arm between the second and the third strand are presented in Figure 8B. In the X-ray study no electron density was

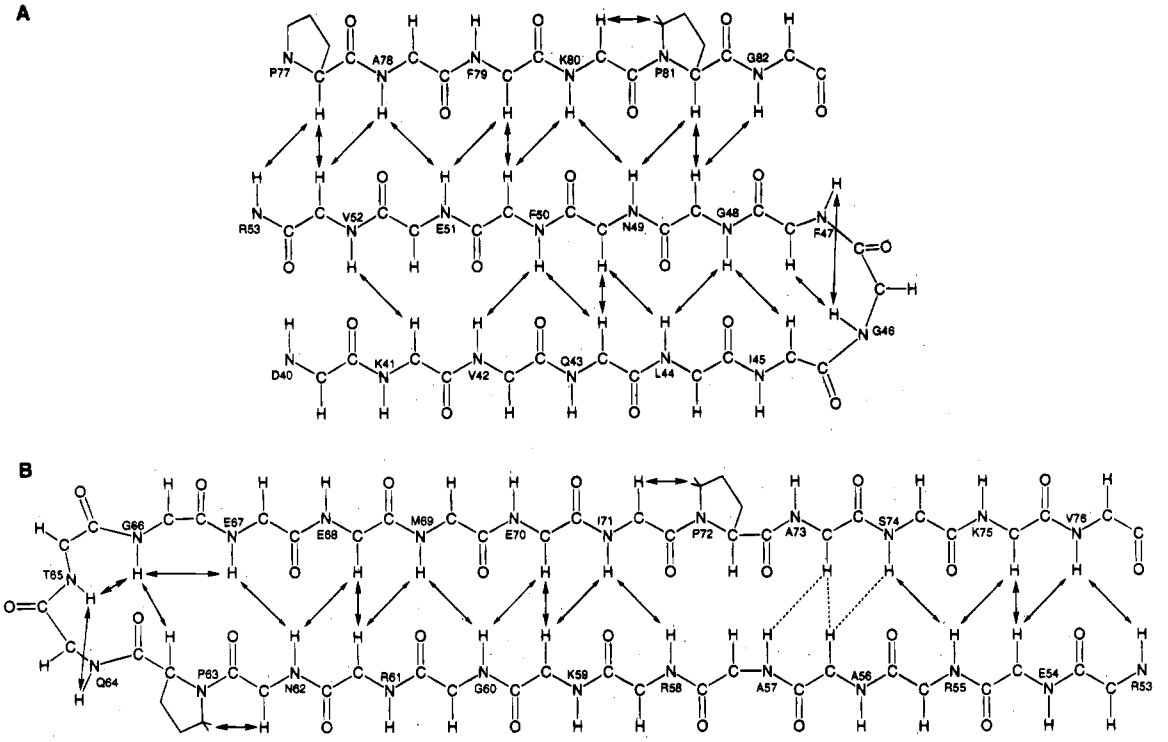

FIGURE 8: Schematic arrangement of the three-stranded antiparallel β-sheet (A) and of the DNA-binding arm (B) of HUBst based on short-distance long range backbone-to-backbone NOEs. The dashed lines at A57 and A73 indicate that the unambiguous NOE assignment was very difficult due to overlap of both the $^1H^\alpha$ and the $^{13}C^\alpha$ chemical shifts.

observed beyond residues Ala-57 and Ala-73 (White et al., 1989). The remainder of the arm was modeled as a regular extension of the β-sheet. Surprisingly, a different structure results from our NMR data. As shown in Figure 8B a regular antiparallel β-sheet is observed from residues Arg-53 to Ala-56 and Ala-73 to Val-76, as also seen in the X-ray structure. Then, at Ala-57 and at Pro-72 the strands flip inside out and continue as a regular antiparallel β-sheet up to Pro-63 and Glu-67. Here again, the strands flip over at Pro-63 and Gly-66. After this, a regular type I β-turn was observed involving Pro-63 to Gly-66, as evidenced by the intermediate exchange of the amide proton of Gly-66 and by two consecutive strong sequential d_{NN} NOEs between Gln-64 and Thr-65 and between Thr-65 and Gly-66 in combination with a weak $d_{\alpha N}$-(i,i+3) NOE between Pro-63 and Gly-66, as shown in Figure 7.

For proline residues in a type I β-turn the second position is statistically the most favorable position (Wilmot et al., 1988; Sibanda et al., 1989), and in such a case the cis form of the peptide bond between the proline and the preceding residue is preferred. However, equally strong NOEs observed between $^1H^\alpha$ of Asn-62 and both $^1H^{\delta1}$ and $^1H^{\delta2}$ of Pro-63 indicate that the trans form is adopted, which indeed is required for the first position of a type I turn. The same sequential NOEs were observed for Pro-72, Pro-77, and Pro-81, indicating a trans form of the corresponding peptide bonds. All prolines of HUBst are involved in changes of the β-ribbon structure: Pro-63 introduces a turn, Pro-72 attributes to the distortion of the β-ribbon, Pro-77 terminates the β-arm, and Pro-81 introduces the structural transition to the third α-helix.

Previously (Tanaka et al., 1984), the DNA-binding arms of HU were modeled, which suggested that the "outgoing" strand would contain 11 residues and the "return" strand 13 residues, where position 63 would occupy position 2 of a β-turn at the end of the arm. However, the present NMR study demonstrates that in the solution structure of HUBst Pro-63 occupies position 1 of a type I β-turn, which implies that the "outgoing" and the "return" strand both consist of 12 residues.

CONCLUDING REMARKS

In the present paper the complete assignment of the ^1H, ^{13}C, and ^{15}N nuclear magnetic resonances of the protein HU from *B. stearothermophilus* in solution is reported. This provides a starting point for NMR studies of its structure, dynamics, and the mode of DNA binding. The secondary structure was determined based on a qualitative analysis of NOE data derived from one 3D NOESY-(^{13}C,^{15}N)-HSQC spectrum, on $^1H^\alpha$, $^1H^N$, $^{13}C^\beta$, $^{13}C^\alpha$, ^{13}CO, and ^{15}N chemical shifts and on amide proton exchange data. The arrangement of the three α-helices and the three extended strands was found to be consistent with the X-ray structure. However, the second α-helix in the solution structure begins three residues earlier, and consequently the loop between the first two α-helices is shorter. Furthermore, the conformation of the end of the β-arm region is different from that suggested previously (Tanaka et al., 1984; White et al., 1989). A study to determine the three-dimensional structure of the HUBst dimer in solution is currently in progress.

SUPPLEMENTARY MATERIAL AVAILABLE

A summary of NMR parameters used in the NMR experiments recorded for HUBs is available (2 pages). Ordering information is given on any current masthead page.

REFERENCES

Bax, A., & Pochapsky, S. (1992) *J. Magn. Reson. 99*, 638–643.

Bax, A., Ikura, M., Kay, L. E., Torchia, D. A., & Tschudin, R. (1990a) *J. Magn. Reson. 86*, 304−318.
Bax, A., Clore, G. M., Driscoll, P. C., Gronenborn, A. M., Ikura, M., & Kay, L. E. (1990b) *J. Magn. Reson. 87*, 620−627.
Bax, A., Clore, G. M., & Gronenborn, A. M. (1990c) *J. Magn. Reson. 88*, 425−431.
Boelens, R., Burgering, M. J. M., Fogh, R., & Kaptein, R. (1994) *J. Biomol. NMR 4*, 201−213.
Brown, S. C., Weber, P. L., & Mueller, L. (1988) *J. Magn. Reson. 77*, 166−169.
Clore, G. M., Bax, A., Driscoll, P. C., Wingfield, P T., & Gronenborn, A. M. (1990) *Biochemistry 29*, 8172−8184.
Clubb, R. T., Thanabal, V., & Wagner, G. (1992) *J. Magn. Reson. 97*, 213−217.
Craig, N. L., & Nash, H. A. (1984) *Cell 39*, 707−716.
Drlica, K., & Rouviere-Yaniv, J. (1987) *Microbiol. Rev. 51*, 301−319.
Dijk, J., White, S. W., Wilson, K. S., & Appelt, K. (1983) *J. Biol. Chem. 258*, 4003−4006.
Farmer, B. T., II (1991) *J. Magn. Reson. 93*, 635−641.
Goodman, S., Yang, C., Nash, H., Sarai, A., & Jernigan, R. (1990) *Structure & Methods,* Proceedings of the Conversation in the Discipline Biomolecular Stereodynamics, 6th, 1989, Vol. 2, pp 51−62, Adenine Press.
Grzesiek, S., & Bax, A. (1992) *J. Magn. Reson. 96*, 432−440.
Grzesiek, S., & Bax, A. (1993a) *J. Biomol. NMR 3*, 185−204.
Grzesiek, S., & Bax, A. (1993b) *J. Magn. Reson. B 102*, 103−106.
Härd, T., Sayre, M. H., Geiduschek, E. P., & Kearns, D. R. (1989) *Biochemistry 28*, 2813−2819.
Hurd, R. E. (1990) *J. Magn. Reson. 87*, 422−428.
Ikura, M., Kay, L. E., & Bax, A. (1990) *Biochemistry 29*, 4659−4667.
Kay, L. E. (1993) *J. Am. Chem. Soc. 115*, 2055−2057.
Kellenberger, E., (1988) *Biophys. Chem 29*, 51−62.
Kimura, K., & Wilson, K. S. (1983) *J. Biol. Chem. 258*, 4007−4011.
Kleywegt, G. J., Vuister, G. W., Padilla, A., Knegtel, R. M. A., Boelens, R., & Kaptein, R. (1993) *J. Magn. Reson. B 102*, 166−176.
Lammi, M., Paci, M., & Gualerzi, C. B. (1984) *FEBS Lett. 170*, 99−104.
Marion, D., & Wüthrich, K. (1983) *Biochem. Biophys. Res. Commun. 113*, 967−974.
Marion, D., Kay, L. E., Sparks, S. W., Torchia, D. A., & Bax, A. (1989a) *J. Am. Chem. Soc. 111*, 1515−1517.
Marion, D., Ikura, M., Tschudin, R., & Bax, A. (1989b) *J. Magn. Reson. 85*, 393−399.
McGhee, J., & Felsenfeld, G. (1980) *Annu. Rev. Biochem. 49*, 1115−1156.
Norwood, T. J., Boyd, J., Heritage, J. E., Soff, N., & Campbell, I. D. (1990) *J. Magn. Reson. 87*, 488−501.
Olejniczak, E. T., & Eaton, H. (1990) *J. Magn. Reson. 87*, 628−632.
Padas, P. M., Wilson, K. S., & Vorgias, C. E., (1992) *Gene 117*, 39−44.
Pardi, A., Wagner, G., & Wüthrich, K. (1983) *Eur. J. Biochem. 137*, 445−454.
Pascal, S. M., Muhandiram, D. R., Yamazaki, T., Forman-Kay, J. D., & Kay, L. E. (1994) *J. Magn. Reson. B 103*, 197−201.
Pelton, J. G., Torchia, D. A., Meadow, N. D., Wong, C., & Roseman, S. (1991) *Biochemistry 30*, 10043−10057.
Powers, R., Garret, D. S., March, C. J., Frieden, E. A., Gronenborn, A., & Clore, G. M. (1992) *Biochemisty 31*, 4334−4346.
Press, W. H., Teukolsky, S. A., Vettering, W. T., & Flannery, B. P. (1992) *Numerical Recipes,* Cambridge University Press, Cambridge, U.K.
Sibanda, B. L., Blundell, T. L., & Thornton, J. M. (1989) *J. Mol. Biol. 206*, 759−777.
Sørensen, O. W. (1990) *J. Magn. Reson. 89*, 210−216.
Spera, S., & Bax, A. (1991) *J. Am. Chem. Soc. 113*, 5490−5492.
Tanaka, I., Appelt, K., Dijk, J., White, S. W., & Wlison, K. S. (1984) *Nature 310*, 376−381.
Vuister, G. W., Boelens, R., Kaptein, R., Hurd, R. E., John, B., & Van Zijl, P. C. M. (1991) *J. Am. Chem. Soc. 113*, 9688−9690.
White, S. W., Appelt, K., Wilson, K. S., & Tanaka, I. (1989) *Proteins 5*, 281−288.
Wilmot, C. M., & Thornton, J. M. (1988) *J. Mol. Biol. 203*, 221−232.
Wilson, K. S., Vorgias, C. E., Tanaka, I., White, S., & Kimura, M. (1990) *Protein Eng. 4*, 11−22.
Wishart, D. S., & Sykes, B. D. (1994) *J. Biomol. NMR 4*, 171−180.
Wishart, D. S., Sykes, B. D., & Richards, F. M. (1991) *J. Mol. Biol. 222*, 311−333.
Wüthrich, K. (1986) *NMR of Proteins and Nucleic Acids*, Wiley, New York.
Yamazaki, T., Yoshida, M., & Nagayama, K. (1993) *Biochemistry 32*, 5656−5669.
Zuiderweg, E. R. P., & Fesik, S. W. (1989) *Biochemistry 28*, 2387−2391.